Fermi National Accelerator Laboratory

FERMILAB-Conf-94/021-E

DØ

Production of W and Z Bosons at DØ

Norman A. Graf
For the DØ Collaboration

Brookhaven National Laboratory
Upton, Long Island, New York 11973

Fermi National Accelerator Laboratory
P.O. Box 500, Batavia, Illinois 60510

January 1994

Presented at the *9th Topical Workshop on Proton-Antiproton Collider Physics*,
Tsukuba, Japan, October 18-22, 1993

Disclaimer

Production of W and Z bosons at DØ

The DØ Collaboration
Presented by Norman A. Graf
Brookhaven National Laboratory
Upton, Long Island, New York USA 11973

Preliminary results from the DØ experiment are presented on production properties of the $W^{\pm}$ and Z^0 gauge bosons using final states containing electrons and muons. The DØ detector has accumulated 16.7 pb^{-1} of data at the Fermilab $\bar{p}p$ Tevatron collider. Based on a subset of this data preliminary measurements of the $W^{\pm}$ and Z^0 production cross section and a measurement of α_s at $Q^2 = M_W^2$ derived from the ratio of W+1jet to W+0jets is presented.

1. Introduction

DØ has been designed to study high p_T physics at the Fermilab $\bar{p}p$ Collider. The detector was commissioned with $\bar{p}p$ collisions during the summer of 1992 and began taking data in August of that year. The data run ended in June 1993 after logging 16.7 pb^{-1} of data. Over 13 million events were accumulated and fully reconstructed for physics analysis. The results presented here are preliminary, and are based on a subset of the full data sample.

The detector elements provide precision measurements of leptons, jets, and missing transverse energy ($\not\!\!E_T$). They consist of a non-magnetic central tracking system, surrounded by a compact calorimeter and a full-coverage muon system. The detector has been described in detail elsewhere [1], however, those aspects which are relevant for this analysis are presented here for reference.

1.1 The DØ Detector

The inner tracking system covers a cylindrical region of radius 75 *cm* and 3 *m* in length with wire gas drift chambers to detect charged tracks in a pseudorapidity range of $|\eta| < 3$ with full azimuthal coverage. The chambers provide the primary interaction vertices and track directions for charged lepton candidates as well as a measure of dE/dx along the track. An additional three–layer cylindrical transition radiation detector aids in electron identification over a range $|\eta| < 1.2$.

The absence of a central magnetic field allows the calorimeter to be compact and enhances the hermeticity of its coverage. The calorimeter is a uranium–liquid argon sampling detector, contained within a central cryostat and two end cryostats which provide coverage over the range $|\eta| \sim 4$. The electromagnetic section is 21 radiation lengths (X_0) deep and has a fractional energy resolution of $15\%/\sqrt{E[GeV]}$. The measured EM calorimeter response is linear to within 0.5% over the energy range 10–150 GeV [2]. The hadronic section is 7–9 interaction lengths (λ) thick and has a measured fractional energy resolution for pions of $50\%/\sqrt{E}$ [3]. The calorimeter readout is based on finely segmented (0.1×0.1

$\eta \times \phi$) pseudo-projective towers. This is further subdivided to 0.05×0.05 cells in the third EM calorimeter depth (shower maximum) offering fine spatial resolution for electromagnetic showers. The region between the cryostats has been instrumented with tiles of scintillator (Intercryostat Detector or ICD) to correct for energy deposits which would not be detected by the calorimeter itself. In addition, separate single cell readouts are installed in the edges of the calorimeters to sample showers induced by the cryostat walls. Together, the ICD and massless gaps provide a good approximation to the standard DØ sampling of showers in the transition region between the calorimeters.

The muon system is located outside the calorimeter cryostats. It consists of three layers of chambers with magnetized iron toroids located between the first and second layers. The inner layer consists of four planes of proportional wire drift tubes, while the outer chambers have three planes each. The bend coordinate is measured by the drift time, while the non-bend coordinate is measured by the time difference of the signal read out of each end of the wire, refined by a vernier cathode pad charge ratio. The magnetic field in the iron toroid is 1.9 Tesla, providing momentum measurement with a design resolution of $\sigma(p)/p = 0.2 \oplus 0.001p$ as well as charge discrimination up to 350 GeV/c. The thickness of the calorimeter plus iron toroids varies from 14 λ in the central region to 19 λ in the forward region.

2 W and Z Decays to Muons

2.1 Triggering

DØ employs a multilevel trigger to select events of interest. The initial trigger (Level 0) simply requires a hard scatter to be detected in two scintillator hodoscopes placed on either side of the interaction vertex. The next level trigger (Level 1) employs fast hardware signals to make a decision. For the central muon system ($|\eta| < 1.7$), hits in two of three layers within a wide road are sufficient to trigger. This is refined in a Level 1.5 trigger which requires all three layers to have hits within a finer road. This imposes an effective 7 GeV/c p_T threshold. Finally a Level 2 software trigger imposes cuts which are essentially the same as those imposed offline. Additionally, cosmic ray rejection based on the event topology is implemented. One requires a single muon above 15 GeV/c p_T for the W trigger and two muons above 10 GeV/c p_T for the Z trigger.

2.2 Muon Identification

The offline muon selection was based on the following series of cuts. A loose muon was required to possess a good quality reconstructed track in the muon chambers. Additionally, tight muon cuts required the track to pass through a minimum length of magnetized iron. This assured a good momentum measurement and reduced the backgrounds from the cracks between the central and end muon systems. The track was then projected into the calorimeter where the energy deposition along the muon direction was required to be isolated and consistent with a minimum ionizing particle. A matching track was required to be reconstructed in the central tracking chambers. Furthermore this track was required to originate from the primary interaction vertex by imposing impact parameter cuts of 25 cm in the 3D

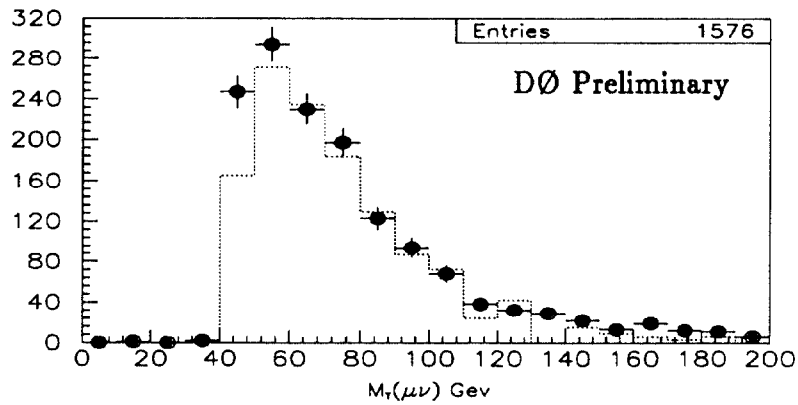

Figure 1: The transverse mass distribution for $W^{\pm} \rightarrow \mu^{\pm}\nu$. The points represent the data while the histogram is the MC prediction, normalized to the expected net signal.

view and 10 cm in the non-bend transverse view.

2.3 W and Z Production Cross Sections

The analysis was based on a data sample of 7.3 ± 0.9 pb^{-1}. The W event selection required the presence of one muon passing the tight requirements having p_T greater than 20 GeV/c and $\not\!\!E_T$ of at least 20 GeV in the event. Topological cuts to remove cosmic rays were also applied. The Z event sample was selected requiring at least one muon passing the tight requirements and another muon on which these requirements were relaxed. The kinematic cuts required one muon above 20 GeV/c p_T , the other above 15 GeV/c. To remove the backgrounds from cosmic rays, back-to-back muons were removed and low mass dimuons were also rejected by requiring a minimum opening angle of 30°.

Applying the above cuts results in a data sample containing 1576 W candidates and 93 Z candidates. The transverse mass, defined as

$$M_T^2 = 2E_T^{\mu}E_T^{\nu}(1 - cos\Delta\phi),$$

where the transverse energy of the neutrino is defined by $E_T^{\nu} = \not\!\!E_T$ for the W candidate events is shown in Figure 1. Superimposed on the data points is a Monte Carlo prediction for this distribution, normalized to the number of W events expected after background subtraction. In Figure 2 is shown the invariant mass distribution for the $Z^0 \rightarrow \mu^+\mu^-$ event sample. Again, the superimposed histogram is the Monte Carlo distribution normalized to the number of Z signal events expected after background subtraction.

The QCD and cosmic ray background contributions to the above processes have been estimated from the data. The W background contributions from physics sources such as $Z^0 \rightarrow \mu^+\mu^-$ where one muon is lost or $W^{\pm} \rightarrow \tau^{\pm}\nu$ where the τ subsequently decays into $\mu\nu_{\mu}\nu_{\tau}$ have been estimated from Monte Carlo simulations. The primary source of backgrounds to the $Z^0 \rightarrow \mu^+\mu^-$ sample is cosmic rays, with other sources contributing negligibly.

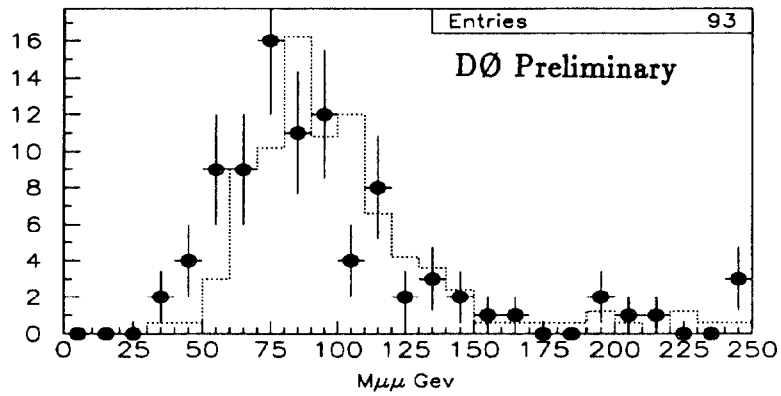

Figure 2: The $\mu\mu$ invariant mass distribution for $Z^0 \to \mu^+\mu^-$. The points represent the data while the histogram is the MC prediction, normalized to the expected net signal.

The estimated values for these backgrounds can be found in Table 1. Also to be found in Table 1 are the calculated acceptances and efficiencies for the W and Z selection. These values were derived from a mixture of Monte Carlo studies and an analysis of the data itself.

	$W^{\pm} \to \mu^{\pm}\nu$	$Z^0 \to \mu^+\mu^-$
Acceptance(%)	22.1 ± 1.2	26.7 ± 2.3
Offline selection(%)	37.2 ± 7.0	22.5 ± 5.3
Total Efficiency(%)	$\mathbf{8.2 \pm 1.6}$	$\mathbf{6.0 \pm 1.6}$
Signal	1576 ± 40	93 ± 10
Est. Background(%)	24 ± 4	6 ± 3
Net Signal	$\mathbf{1198 \pm 44 \pm 62}$	$\mathbf{87 \pm 10 \pm 3}$

Table 1: Efficiencies and acceptances for W and Z decays into muons.

Preliminary values for the W and Z cross section times branching ratio into muons can be derived from the data presented in Table 1. The values are:

$$\sigma \cdot \mathrm{B}(\mathrm{W}^{\pm} \to \mu^{\pm}\nu) \;=\; 2.00 \pm 0.07(\mathrm{stat}) \pm 0.41(\mathrm{sys}) \pm 0.24(\mathrm{lum})\ \mathrm{nb}$$

and

$$\sigma \cdot \mathrm{B}(\mathrm{Z}^0 \to \mu^+\mu^-) \;=\; 0.20 \pm 0.02(\mathrm{stat}) \pm 0.05(\mathrm{sys}) \pm 0.02(\mathrm{lum})\ \mathrm{nb}.$$

The uncertainty due to the luminosity measurement can be eliminated by taking the ratio of the two measurements. This ratio can also be used to extract further information from the data as will be discussed in the next section. The preliminary measurement of the ratio R_μ is:

$$\mathrm{R}_\mu \;\equiv\; \frac{\sigma \cdot \mathrm{B}(\mathrm{W}^{\pm} \to \mu^{\pm}\nu)}{\sigma \cdot \mathrm{B}(\mathrm{Z}^0 \to \mu^+\mu^-)} \;=\; 10.0 \pm 1.1(\mathrm{stat}) \pm 2.4(\mathrm{sys}).$$

3 W and Z Decays to Electrons

3.1 Triggering

The data for the cross section analysis of W and Z bosons decaying into electrons were accumulated under a common single electron trigger. This was motivated by a desire to reduce the systematic uncertainties in the measurement of the ratio of the cross sections, where errors due to the trigger efficiency calculations partially cancel.

The electron Level 1 trigger simply requires a single calorimeter trigger tower (0.2×0.2 in $\eta \times \phi$) above a threshold of 10 GeV E_T or two towers above 7 GeV E_T . The Level 2 software trigger applies transverse and longitudinal shape cuts to the electromagnetic clusters as well as imposing isolation criteria. The W and Z cross section analysis was based on a single–electron trigger above 20 GeV E_T .

3.2 Electron Identification

Electron candidates are identified in the offline reconstruction by forming nearest–neighbor clusters of EM calorimeter readout towers. The offline selection criteria for electron identification then consist of:

- Cluster Electromagnetic Energy Fraction
- Cluster Shape χ^2 cut
- Cluster Isolation
- Cluster–Track Match Significance

The first cut simply requires that 90% of the cluster energy be contained within the EM calorimeter. The electromagnetic calorimeter being 21 X_0 thick makes this a highly efficient cut.

The cluster shape is then required to be consistent with that of an electron. This is imposed as a cut on the cluster χ^2 determined from the energy distribution within the cluster. The transverse and lateral energy deposition of both testbeam and Monte Carlo electrons is measured and a covariance matrix is constructed from these measurements. The matrix contains the average energy deposited in each calorimeter cell as well as its variance and its covariance with energies deposited in neighboring cells. The covariance matrix contains both energy and η dependencies. For each event, the measured energy depositions for an electron candidate are compared with that expected from the reference sample and a χ^2 quantity is constructed. The χ^2 for 41 degrees of freedom is required to be less than 100 in the central region and 200 in the forward calorimeters.

The cluster is then required to be isolated from other sources of energy in the events. The isolation variable is defined as the ratio $(E(0.4) - EM(0.2))/EM(0.2)$. The total energy in a cone defined by a radius $\sqrt{\Delta\eta^2 + \Delta\phi^2} < 0.4$ centered on the electron is denoted by $E(0.4)$ while $EM(0.2)$ is the electromagnetic energy in a cone of radius 0.2. The cut is effectively

requiring the electron energy to be deposited within a cone of 0.2 and to be isolated within a cone of 0.4 from other particles in the event. The isolation was required to be less than 0.15.

Finally, the calorimeter cluster is required to be well matched to a reconstructed central track. The cluster centroid is determined from the calorimeter energy deposition and the track parameters are extrapolated to the shower position. The track matching significance is defined as $\sqrt{(R\Delta\phi/\sigma(R\Delta\phi))^2 + (\Delta z/\sigma(\Delta z))^2)}$, where $R\Delta\phi$ and Δz are the differences between the measured centroid and projected track positions. The significance variable was required to be less than 10.

3.3 W and Z Production Cross Sections

The analysis was based on a data sample of 7.58 ± 0.91 pb^{-1}. The W candidate sample was selected by requiring the presence of one electron passing all the previously described cuts as well as fiducial cuts restricting them to well-measured regions of the detector. The kinematic cuts required the electron $E_T > 25$ GeV as well as $\not\!\!E_T > 25$ GeV. The Z selection required two electrons with $E_T > 25$ GeV. The absolute energy scale of the EM calorimeters for this analysis was set by scaling the invariant mass peak to the LEP value for the Z mass [4]. Detailed descriptions of the energy scale and its effect on the W mass measurement can be found in the following talk [5].

Table 2 summarizes the efficiencies, acceptances and backgrounds for this analysis. The trigger efficiencies have been derived from an unbiased independent trigger. The backgrounds for the W sample have been estimated from the data and Monte Carlo studies whereas the background under the Z invariant mass peak has been estimated by interpolating the sideband contributions into the signal region (defined to be 71 GeV $< M_{ee} <$ 111 GeV). The final data sample contained 5846 W and 326 Z candidates. The transverse mass of the W for this data sample is shown in Figure 3 and the invariant mass of the Z events can be found in Figure 4.

	$W^{\pm} \rightarrow e^{\pm}\nu$	$Z^0 \rightarrow e^+e^-$
Geometrical Acceptance(%)	47.1 ± 1.0	37.2 ± 0.7
Trigger Efficiency(%)	98.6 ± 1.2	99.9 ± 0.2
Offline Selection(%)	74.1 ± 2.0	54.9 ± 3.0
Total Efficiency(%)	$\mathbf{34.4 \pm 2.5}$	$\mathbf{20.4 \pm 1.2}$
Signal	6314 ± 80	337 ± 18
Est. Background(%)	7.4 ± 2.0	3.3 ± 1.8
Net Signal	$\mathbf{5846 \pm 166}$	$\mathbf{326 \pm 19}$

Table 2: Efficiencies and acceptances for W and Z decays into electrons.

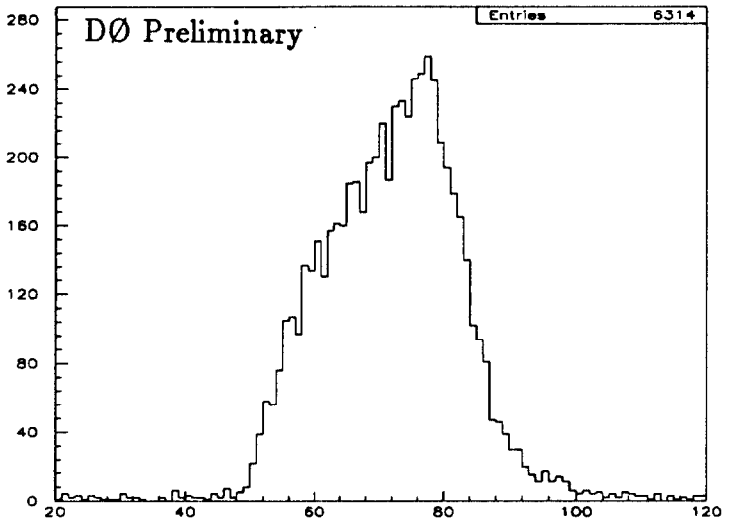

Figure 3: The transverse mass distribution for $W^{\pm} \rightarrow e^{\pm}\nu$. The energy scale was set using the mass of the Z boson.

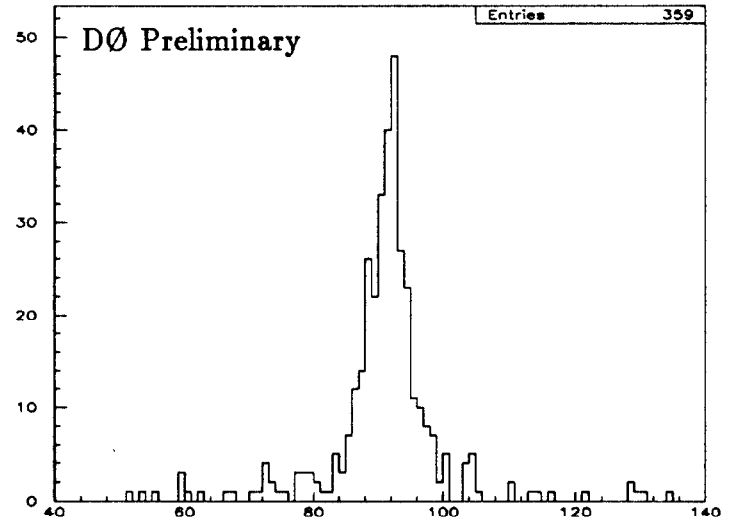

Figure 4: The ee invariant mass distribution for $Z^0 \rightarrow e^+e^-$ candidates. The energy scale was set using the mass of the Z boson.

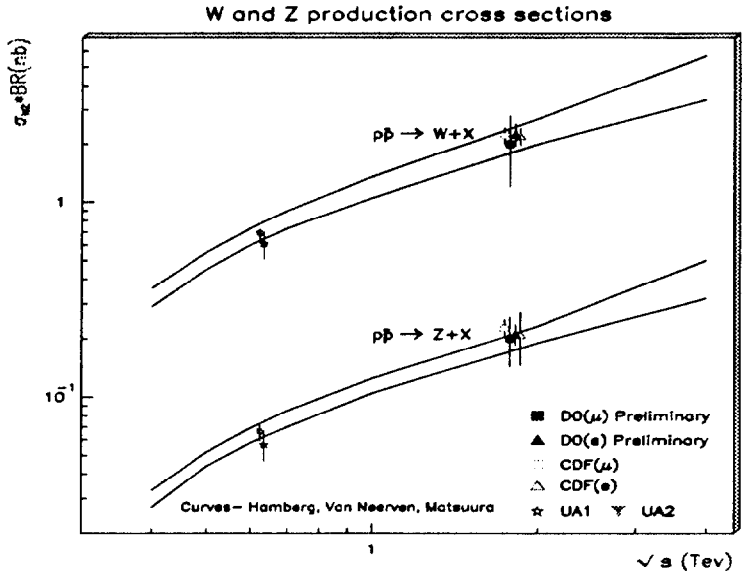

Figure 5: Preliminary W and Z production cross sections as measured by DØ compared with previous experimental measurements and theoretical predictions.

Accounting for the acceptances and efficiencies of the selection gives the following values for the W and Z cross section times branching ratio into electrons:

$$\sigma \cdot \mathrm{B}(\mathrm{W}^{\pm} \rightarrow \mathrm{e}^{\pm}\nu) \;=\; 2.25 \pm 0.03(\mathrm{stat}) \pm 0.10(\mathrm{sys}) \pm 0.27(\mathrm{lum})\ \mathrm{nb}$$

and

$$\sigma \cdot \mathrm{B}(\mathrm{Z}^{0} \rightarrow \mathrm{e}^{+}\mathrm{e}^{-}) \;=\; 0.21 \pm 0.01(\mathrm{stat}) \pm 0.01(\mathrm{sys}) \pm 0.02(\mathrm{lum})\ \mathrm{nb}.$$

These values are compared with the theoretical predictions [6] as well as published results from other experiments in Figure 5.

3.3 R, Γ_W and top mass limit

The largest sources of uncertainty in the measurements of the cross sections themselves are the systematic uncertainties in the efficiency and luminosity calculations. Although these uncertainties are expected to diminish as the analyses mature, one can reduce the effect of these uncertainties by measuring the ratio of the cross sections, since some of the errors are common to both measurements. The uncertainty in the luminosity measurement cancels completely and the errors on the selection efficiency and acceptance cancel partially. The preliminary value of this ratio is:

$$\mathrm{R_e} \;\equiv\; \frac{\sigma \cdot \mathrm{B}(\mathrm{W}^{\pm} \rightarrow \mathrm{e}^{\pm}\nu)}{\sigma \cdot \mathrm{B}(\mathrm{Z}^{0} \rightarrow \mathrm{e}^{+}\mathrm{e}^{-})} \;=\; 10.70 \pm 0.60(\mathrm{stat}) \pm 0.50(\mathrm{sys}).$$

This ratio is of interest for other reasons as well since it can be expressed as the following combination of precisely measureable or calculable quantities:

$$R_e \equiv \frac{\sigma \cdot \mathrm{B}(W^{\pm} \rightarrow e^{\pm}\nu)}{\sigma \cdot \mathrm{B}(Z^{0} \rightarrow e^{+}e^{-})} = \frac{\Gamma(W^{\pm} \rightarrow e^{\pm}\nu)}{\Gamma(W)} \cdot \frac{\Gamma(Z)}{\Gamma(Z^{0} \rightarrow e^{+}e^{-})} \cdot \frac{\sigma(\bar{p}p \rightarrow W^{\pm})}{\sigma(\bar{p}p \rightarrow Z^{0})}.$$

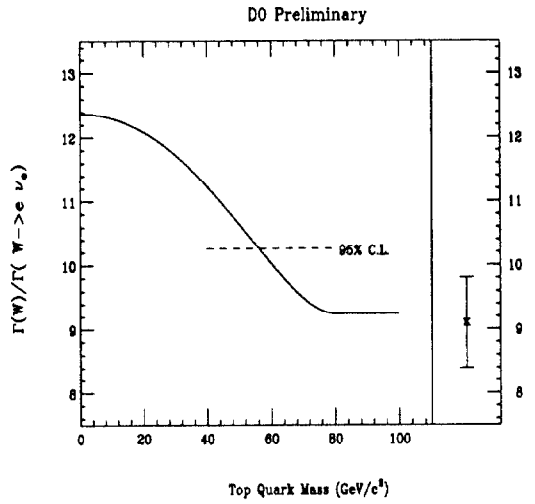

Figure 6: The ratio $\Gamma(W)/\Gamma(W^{\pm} \rightarrow e^{\pm}\nu)$ as a function of the top quark mass for $M_W = 80.0$ GeV/c^2 and $\alpha_s = 0.13$.

To extract a measurement of the total width of the W, $\Gamma(W)$ from the measurement of R we use the LEP measurement for the Z width, $\Gamma(Z) = 2.487 \pm 0.010$ GeV[4]. For the ratio of the W and Z leptonic decay widths we take the theoretical value, $\Gamma(W^{\pm} \rightarrow e^{\pm}\nu)/\Gamma(Z^0 \rightarrow e^+e^-) = 2.70 \pm 0.02$[7]. The ratio of W to Z production is determined using the calculation of Hamberg, Van Neerven and Matsuura[6], convoluted with various parton distribution functions to obtain $\sigma(\bar{p}p \rightarrow W^{\pm})/\sigma(\bar{p}p \rightarrow Z^0) = 3.26 \pm 0.08$[8]. Combining these numbers with the quoted value of R, we obtain the result $\Gamma(W) = 2.05 \pm 0.16$ GeV. This result can be compared with the Standard Model prediction [9] of $\Gamma(W) = 2.08 \pm 0.02$ GeV for $M_t > M_b + M_W$ where M_t, M_b and M_W are the masses of the top quark, bottom quark and W boson, respectively. For a top quark mass below the W mass, the total width of the W would reflect possible decays into top. A limit on the top quark mass, independent of the top quark decay modes, can therefore be extracted from this measurement. To reduce the sensitivity on the W mass, one uses the ratio $\Gamma(W)/\Gamma(W^{\pm} \rightarrow e^{\pm}\nu)$ in this measurement, for which we have used the value 83.24±0.42 MeV [4]. Figure 6 shows a prediction for the ratio $\Gamma(W)/\Gamma(W^{\pm} \rightarrow e^{\pm}\nu)$ as a function of the top quark mass, together with the preliminary DØ result for $\Gamma(W)/\Gamma(W^{\pm} \rightarrow e^{\pm}\nu) = 9.10 \pm 0.71$. The 95% confidence level lower limit on the top mass is then 56 GeV/c^2.

4. Measurement of α_s

Recent advances in the theoretical understanding of the production of W bosons coupled with the increase in the amount of experimental data make it possible to make more precise comparisons between theoretical predictions and experimental measurements. Measuring the ratio of events containing a W boson accompanied by one jet to the number with no associated jets allows one to quantitatively test perturbative QCD calculations and also to attempt to derive a measurement of the strong coupling constant α_s. Details of this analysis may be found in reference [10].

4.1 Theoretical Motivation

Recent improvements in the next–to–leading order (NLO) theoretical calculations of W + 0 jets [11] and W + 1 jet cross sections have been incorporated into the Monte Carlo program DYRAD [12]. For the purpose of this analysis, the program was modified to provide parameterized forms of the cross sections which explicitly factored out the dependence on α_s, *viz.*

$$\sigma_{W+0j}(NLO) = A_0 + \alpha_s A_1(E_T^{min})$$

$$\sigma_{W+1j}(NLO) = \alpha_s B_0(E_T^{min}) + \alpha_s^2 B_1(E_T^{min}, R).$$

The parameters A_0, $A_1(E_T^{min})$, $B_0(E_T^{min})$, and $B_1(E_T^{min}, R)$ are given as functions of the jet minimum E_T and the cone size of the jet (R); as coefficients of the cross sections they are independent of α_s. To allow for a direct comparison between the prediction and the measurement, DYRAD was further modified to incorporate features of the DØ detector, such as the jet definition, energy resolution and detector acceptance. Also incorporated were the ability to simulate the lepton selection criteria such as isolation. Biases introduced by the selection cuts applied to the data could therefore be minimized.

4.2 Triggering

The data for this analysis were accumulated using a trigger requiring one isolated electron with $E_T > 20$ GeV and $\not\!\!E_T > 20$ GeV, and so differs slightly from the cross section data sample. Since the rate for this trigger was sufficiently low, these data were separated into a special, high–priority data stream which could be processed very quickly. The results are based on 14.3 ± 1.7 pb^{-1} of data.

4.3 Jet Identification

Jets are identified at DØ using a variety of algorithms. The present analysis is based on a fixed-cone algorithm. One starts with an E_T ordered list of calorimeter readout towers. Preclusters are then formed from contiguous towers within a radius R < 0.3, where R = $(\sqrt{\Delta\eta^2 + \Delta\phi^2})$. One computes the jet η, ϕ using the E_T weighted mean of the towers. All the towers within a radius R = 0.7 about this position are then summed to provide a new jet η, ϕ position. This is iterated until the position is stable. Jets are then split or merged if they overlap other jets, and jets with $E_T < 8$ GeV are dropped. The nominal jet E_T is the sum of the constituent cell energies. The absolute jet energy scale is essentially determined from E_T balance in two–jet events, where one of the jets has fluctuated into a highly electromagnetic final state, or where one of the jets is a direct photon from the hard scattering. The electromagnetic response is very well measured at DØ and the overall scale is set by calibrating to the LEP Z mass value [4]. The current systematic uncertainty in the hadronic jet energy scale is estimated to be ~6%. Further details can be found in reference [13].

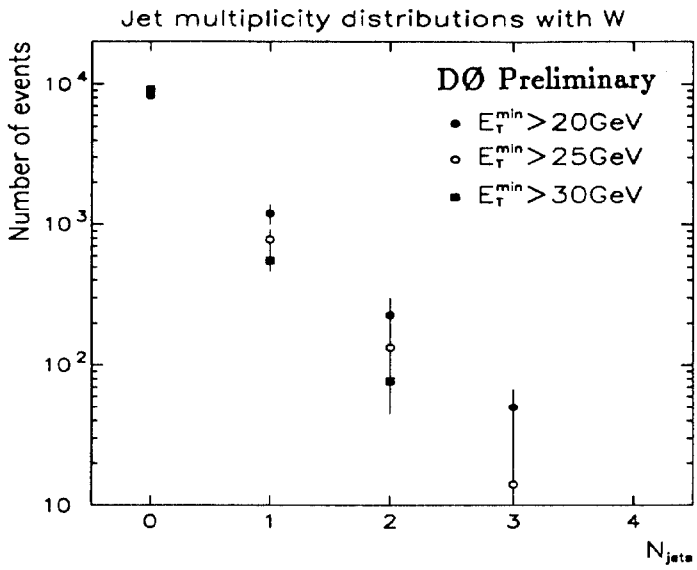

Figure 7: Jet multiplicity distributions as a function of the jet minimum E_T cut (E_T^{min}).

4.4 The Ratio σ(W + 1 jet) / σ(W + 0 jets), α_s and comparison to theory.

The data sample was selected using the same cuts as described in the previous section. The total efficiency for all the cuts, including the trigger, was (33.1±1.1)%, giving a candidate sample of 9770 events. Figure 7 shows the Jet multiplicity distributions as a function of the jet minimum E_T cut (E_T^{min}). The experimental determination of the ratio σ(W + 1 jet) / σ(W + 0 jets) is seen to be strongly affected by the choice of the minimum E_T required for the jet definition. The effect of uncertainties in the energy scale is magnified in the number of jets which are determined to fall above or below any threshold. Figure 8 shows the distribution of the ratio of the number of the W + 1 jet and W + 0 jets events as a function of the minimum jet E_T . The errors on the data points are the statistical uncertainties and the systematic errors due to energy scale added in quadrature. The solid lines in Figure 8 are the next-to-leading order theoretical predictions of the ratio and the dotted lines are the leading order predictions. The theoretical predictions are calculated with two different α_s values to show the sensitivity of the ratio to α_s. The two sets of theoretical predictions show significant differences; the global behavior of the ratio as a function of E_T^{min} shows changes both in the absolute normalization and a weak dependence of the slope on α_s. These variations can, in principle, provide a measure of the strong coupling constant. The behavior of the ratio can also be a measure of uncomputed higher order (next-to-next-to-leading order or higher) corrections. This, of course, will require a more precise experimental measurement.

Using the parameterized expressions for the cross sections returned by DYRAD along with the experimentally measured ratio of the number of W + 1 jet to W + 0 jets events, one can extract a measured value for α_s. As mentioned previously, the experimentally measured ratio is sensitive to the minimum jet E_T , whereas the value of α_s should be independent of E_T^{min}. Figure 9 shows the measured values of α_s as a function of E_T^{min}. In order to maximize the signal statistics and minimize the sensitivity to the jet energy scale uncertainty, the value

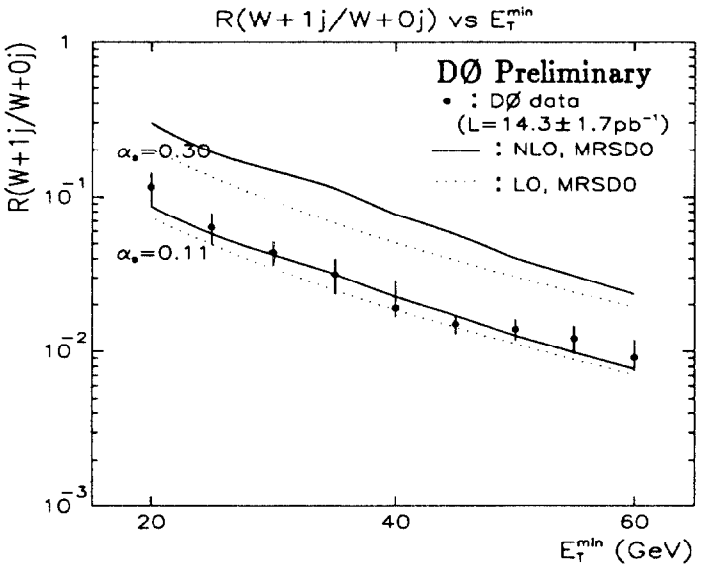

Figure 8: The ratio of the number of W + 1 jet to W + 0 jets events *vs. jet* E_T^{min}.

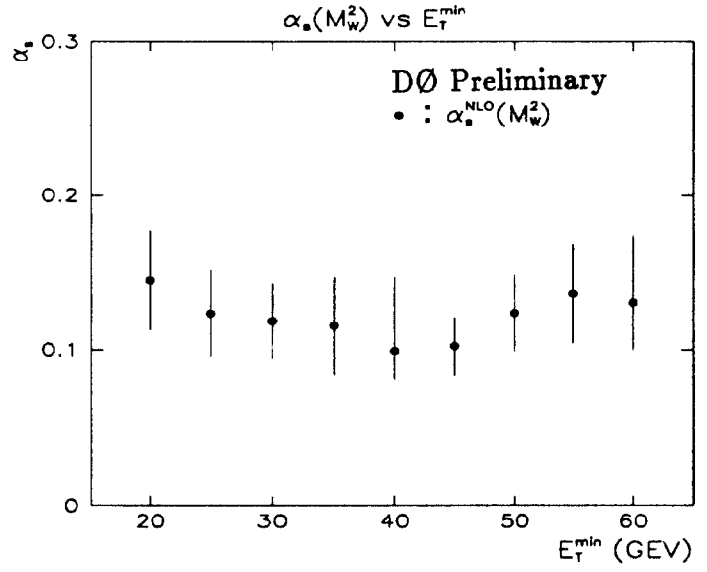

Figure 9: Measured values of α_s as a function of E_T^{min}.

of α_s was extracted at $E_T^{min} = 25$ GeV. The preliminary value for α_s at $Q^2 = M_W^2$ is:

$$\alpha_s^{NLO}(M_W^2) = 0.124 \pm 0.005(stat) \pm 0.006(MC) \pm 0.008(F_{st})^{+0.026}_{-0.022}(Escale)$$

The uncertainty in this measurement is seen to be dominated by the jet energy scale uncertainty. The Monte Carlo error arises solely from the limited event sample used and can be made vanishingly small. F_{st} represents the uncertainty due to the structure functions used.

5. Conclusions

The rather large cross sections for W and Z boson production at the Fermilab Tevatron collider, combined with the unmistakeable experimental signatures of their decays enables precision measurements of these processes at DØ . We have presented measurements of $\sigma \cdot B$ for W and Z boson production and subsequent decays to electrons and muons which are in good agreement with both previous experimental measurements as well as theoretical predictions. Furthermore, the measurement of the total width of the W, extracted from the electron channel, is consistent with Standard Model expectations assuming a heavy top quark, and has been used to set a decay–mode–independent lower mass limit on the top quark mass.

The present state of theoretical understanding of the processes of W plus associated jet production, coupled with the large sample of experimental data has motivated a quantitative comparison of NLO predictions for the ratio of W + 1 jet / W + 0 jets with the experimetally measured value. Although the present experimental systematic uncertainties preclude a rigorous quantitative conclusion, a value for the strong coupling constant, α_s, was extracted from the data. This value is in good agreements with other measurements [14].

The experimental systematic uncertainties, which dominate the measurement errors, are expected to be considerably reduced as the understanding of the detector improves. Additionally, the DØ detector expects to accumulate an additional factor of three to four in integrated luminosity in the near future, significantly improving the statistical and systematic uncertainties. DØ looks forward to fully exploiting the full field of topics available in the electroweak sector.

References

[1] S. Abachi, *et al.*, Fermilab PUB 93/179, to be published in Nucl. Instr. Meth.

[2] H. Aihara, *et al.*, Nucl. Instr. Meth. **A325** 393 (1993).

[3] S. Abachi, *et al.*, Nucl. Instr. Meth. **A324** 53 (1993).

[4] The LEP collaborations: ALEPH, DELPHI, L3 and OPAL, Phys. Lett. **B276**, 247 (1992).

[5] Q. Zhu, "Measurement of the W boson mass in the DØ detector", these proceedings.

[6] R. Hamberg, W.L. Van Neerven and T. Matsuura, Nucl. Phys. **B359** 343 (1991).

[7] W.F.L. Hollik, Fortschr. Phys. **38**, 165 (1990).

[8] S. Lami and D. Wood, DØ Note #1462, July, 1992 (unpublished).

[9] T. Alvarez, A. Leites and J. Terrón, Nucl. Phys. **B301** 1 (1988).

[10] Jaehoon Yu, Ph. D. Thesis, State University of New York at Stony Brook, Stony Brook, NY, 1993 (Unpublished).

[11] H. Baer and M. H. Reno, Florida State report FSU-HEP-901030 (1990).

[12] W. T. Giele, E. W. N. Glover and D. A. Kosower, FERMILAB-Pub-92/230-T, 1992 (To be published).

[13] H. Weerts, "Studies of Jet Production in the DØ Detector", these proceedings.

[14] G. Altarelli, " QCD and Experiment : Status of α_s", CERN-TH.6623/92, 1992 (Unpublished).